

Grain boundary pinning in doped hard sphere crystals†

Volkert W. A. de Villeneuve,^a Leonie Derendorp,^a Danny Verboekend,^a Esther C. M. Vermolen,^b Willem K. Kegel,^a Henk N. W. Lekkerkerker^a and Roel P. A. Dullens^{*c}

Received 1st October 2008, Accepted 5th January 2009

First published as an Advance Article on the web 19th February 2009

DOI: 10.1039/b817255b

Direct visual observations on how grain boundaries are pinned between multiple large spherical impurities during colloidal hard sphere crystallisation are presented. The fluid is stabilized between impurities and acts as a precursor for grain boundary formation. The range of fluid stabilisation by a single impurity is characterized by the frustration length, which goes through a maximum as a function of the impurity-to-particle size ratio. Grain boundaries are more strongly confined to the area between two impurities as the ratio between the impurity-to-impurity spacing and the combined frustration lengths decreases. Our results identify the key parameters in grain boundary formation in doped systems, which may lead to a better control of the grain boundary density in materials.

Introduction

Controlling grain boundary formation is of paramount importance to tailor dynamic and structural material properties to one's needs.^{1–4} For instance, the strength of a material is inversely proportional to the grain size (Hall-Petch effect)^{2,5,6} and transport in materials often occurs in grain boundaries,³ which are relatively disordered and less densely packed compared to the bulk crystal. Also for phenomena like superplasticity and embrittlement^{1–4} it is crucial to control the grain boundary density. This can be achieved by *e.g.* tuning the solidification rate, heating or mechanical annealing.^{3,4,7,8} Another important pathway to tuning the grain boundary density is the insertion of dopants^{9,10} and precipitates^{11,12} – collectively termed impurities.

The simplest conceivable system with impurities is a hard sphere crystal containing larger hard spheres, in which the impurity-to-particle diameter ratio $\alpha \equiv \sigma_i/\sigma_p$ and the volume fraction of impurities ϕ_i are the obvious control parameters. Such a binary system is conveniently realizable using colloids.^{13,14} The intrinsic slowness of colloidal hard spheres and their analogy to atomic systems makes them an excellent model system for material-related studies on the particle level such as nucleation,¹⁵ melting¹⁶ and defect dynamics.^{17–19} Although electron microscopy has provided much of the present experimental knowledge on grain boundaries,^{20–22} colloidal systems have also proved to be useful to address their dynamic properties.^{8,16,18} In our previous work we observed and quantified that *single* impurities collect grain boundaries during crystallisation.^{14,23,24} However, the fundamental question as to why these grain boundaries appeared around impurities remained unsolved. Here, we now identify for

the first time the key conditions under which grain boundaries may appear directly between *multiple* impurities during freezing and remain pinned between them. To this end we consider crystallisation of hard spheres in the presence of multiple impurities and the interaction strength between them.

Experimental

We inserted large hard spherical impurities with α ranging from 3–27 in a supersaturated fluid of otherwise monodisperse hard spheres and compared these to reference samples without impurities. The system consisted of a 0.1 wt% of very large, polydisperse poly(methyl methacrylate) spheres (PMMA) in a suspension of 1.5 μm diameter PMMA particles in two apolar solvent mixtures with nearly matching mass density and refractive index, in which they behave as hard spheres: tetralin, *cis*-decalin and tetrachloromethane,²⁵ and *cis*-decalin/cyclohexylbromide screened with tetrabutyl ammonium bromide.²⁶ Crystallisation proceeded through upward growth from the sample bottom as in ref. 14 at initial particle volume fractions of 0.54–0.55. Imaging was performed with a Nikon Eclipse TE2000U confocal microscope equipped with a Nikon C1 scanning head, at distances of 15–40 μm from the glass sample bottom. Image sequences of 2D *xy*-slices were imaged in the plane of the impurity's center of mass, near impurities with $\alpha = 3–27$, over several hours. Particle coordinates were obtained by methods such as in ref. 27.

Results and discussion

Direct insight into grain boundary formation is gained in real space and time using confocal microscopy. As can be seen in Fig. 1a and b, two crystal fronts approach the fluid between the impurities. As a result, the grain boundary directly forms between the impurities (Fig. 1b), instead of forming and subsequently migrating toward the impurities as was observed in another scenario, *i.e.* by adding impurities in the vicinity of grain boundaries.²⁸ We quantify this process using the local orientational bond order parameter

^aVan 't Hoff Laboratory for Physical and Colloid Chemistry, Utrecht University, Padualaan 8, 3584 CH Utrecht, The Netherlands

^bSoft Condensed Matter, Utrecht University, Princetonplein 1, 3584 CC Utrecht, The Netherlands

^cPhysical and Theoretical Chemistry Laboratory, Department of Chemistry, University of Oxford, South Parks Road, OX1 3QZ Oxford, United Kingdom. E-mail: roel.dullens@chem.ox.ac.uk

† This paper is part of a *Soft Matter* issue highlighting the work of emerging investigators in the soft matter field.

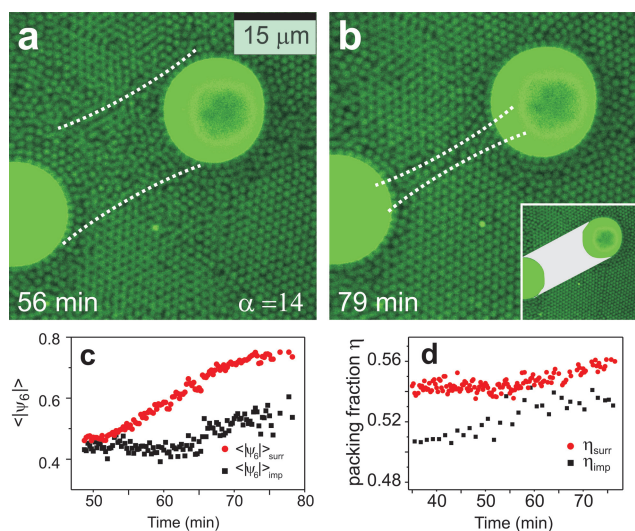


Fig. 1 Grain boundary formation between two impurities with $\alpha = 14$. (a) The fluid bridge between impurities gradually narrows in time and (b) becomes a grain boundary at higher density. The grey area in the inset illustrates the region that was set as the region between the impurities, the rest of the image is considered as surroundings. (c) Evolution of the local hexagonal order between impurities ($\langle |\psi_6| \rangle_{\text{imp}}$) and in the surrounding area ($\langle |\psi_6| \rangle_{\text{surr}}$). Crystallisation between the impurities is clearly retarded. (d) Evolution of the packing fraction between the impurities and in the surrounding area. The packing fraction is systematically lower between the impurities. The points corresponding to the packing fraction between impurities are averaged over five time steps for clarity.

$$\psi_6(\vec{r}) = \frac{1}{N_n} \sum_j^{N_n} e^{6i\theta(\vec{r}_j)},$$

where $|\psi_6| \approx 0.4$ for a typical fluid and $|\psi_6| = 1$ for a perfect hexagonal crystal slice.²⁹ The summation j runs over all N_n next neighbours of a given particle and the angle between the bond vector connecting the particle with next neighbour j and an arbitrary fixed reference axis is defined as $\theta(\vec{r}_j)$. By defining an area between the impurities (inset of Fig. 1b), crystallisation between the impurities ($\langle |\psi_6| \rangle_{\text{imp}}$) and in the surrounding area ($\langle |\psi_6| \rangle_{\text{surr}}$) can be measured separately. The orientational order of the respective areas was calculated as a function of time during grain boundary formation and is shown in Fig. 1c. The rise in $\langle |\psi_6| \rangle_{\text{imp}}$ is clearly delayed compared to $\langle |\psi_6| \rangle_{\text{surr}}$, which confirms the visual observations.

It is quite possible that the two curved impurity surfaces enhance the stability of the fluid, which would lead to the scenario observed in Fig. 1a–c, as the volume fraction of hard sphere fluids near curved surfaces is lowered with respect to the bulk.³⁰ We indeed measure a systematically lower packing fraction $\eta \equiv (N_p \pi \sigma_p^2)/(4A)$ between the impurities, with N_p the number of particles and A the area of interest (Fig. 1d). This effectively results in a ‘fluid bridge’ precursor for grain boundary formation. Eventually, a grain boundary is formed, as the adjacent crystallites tend to have different orientations. The impurities then act as immovable objects that prevents the crystals from reorienting and annealing.³¹ This is in addition to any stabilisation of crystallite orientations along the impurity surface for sufficiently large impurities. The delayed

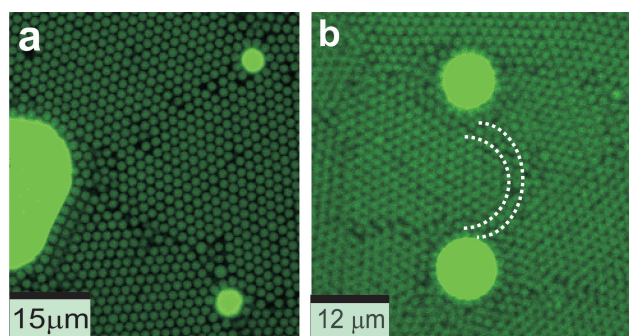


Fig. 2 Factors affecting grain boundary pinning. (a) Impurity spacing: grain boundaries run from impurity to impurity. However, the grain boundaries only appear between the large impurity and the smaller impurities. (b) Impurity size: at similar impurity spacing to Fig. 1b ($\alpha = 14$), grain boundaries are curved for smaller impurities ($\alpha = 6$). The curved lines indicate the shape of the grain boundary.

crystallisation between impurities resembles the reverse process of premelting at grain boundaries.¹⁶

The enhanced fluid stability between impurities provides a thermodynamic argument as to why grain boundaries form there. However, mere visual inspection of additional configurations (Fig. 2) reveals that enhanced fluid stability alone cannot account for these observations. For example in Fig. 2a, grain boundaries are present between the larger impurity and each of the smaller impurities, but no grain boundary has formed between the two smaller impurities, which are at similar distances. Furthermore, in Fig. 2b we observe a strongly curved grain boundary at a similar impurity spacing as in Fig. 1a and b, but between smaller impurities. Hence, the impurity-to-particle size ratio α and impurity-to-impurity (surface-to-surface) spacing L govern the impurity interaction range and strength, which makes them crucial parameters for ‘grain boundary pinning’.

We will now address the effect of α and L on grain boundary pinning, starting by quantifying the range over which a single impurity frustrates the crystal lattice: the ‘frustration length’ ξ . The sum of the frustration lengths of two nearby impurities then gives an estimate of the pair interaction range of nearby impurities. The frustration length is computed by averaging $|\psi_6|$ radially over all particles at distance r from the impurity surface, as well as over typically 10 images to obtain orientational order profiles. Examples of such profiles are shown in Fig. 3a and b for impurities with $\alpha = 3$ and $\alpha = 13$. The corresponding confocal images are shown in Fig. 3c and d. All profiles have initially low orientational order and subsequently rise to a plateau value $\langle |\psi_6| \rangle_{\text{plateau}}$. The frustration length ξ is subsequently obtained by fitting the $\langle |\psi_6| \rangle(r)$ profiles to a plateau fit function

$$\langle |\psi_6| \rangle(r) = \frac{\langle |\psi_6| \rangle_{\text{plateau}}}{1 + b e^{-kr}},$$

with b and k as fit parameters and r in units of σ_p . The length ξ is set such that $\langle |\psi_6| \rangle(\xi) = \kappa \langle |\psi_6| \rangle_{\text{plateau}}$, with $\kappa = 0.95$. The choice for this plateau function and the value for κ are arbitrary and do not affect the results. Note that for smaller impurities $\langle |\psi_6| \rangle$ quickly rises from ~ 0.4 whereas for larger impurities it is initially

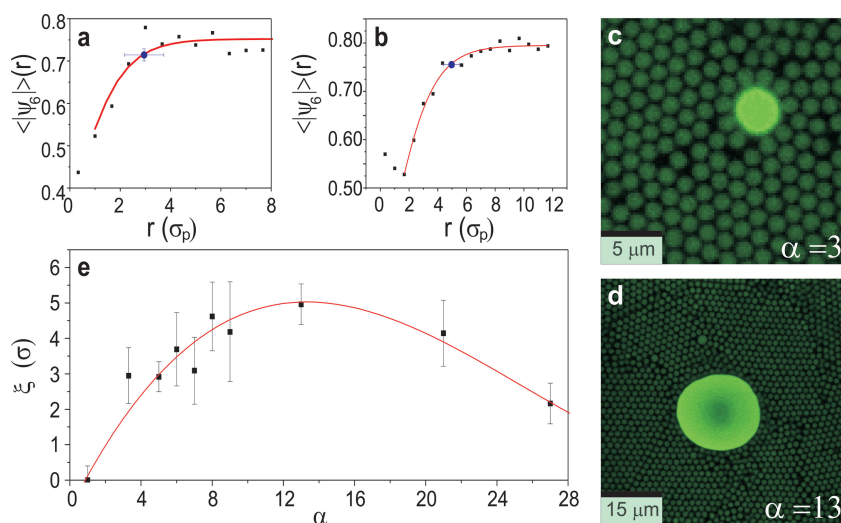


Fig. 3 The frustration length ξ . (a) and (b) Radially and time-averaged $|\psi_6|$ values as a function of distance to the impurity surface for impurities with $\alpha = 3$ (a) and $\alpha = 13$ (b). The obtained ξ values are shown for setting ξ at $\langle |\psi_6| \rangle(r = \xi) = 0.95 \langle |\psi_6| \rangle_{\text{plateau}}$ (filled circles). (c) and (d) The corresponding confocal micrographs for impurities with respectively $\alpha = 3$ (c) and $\alpha = 13$ (d). (e) The frustration length ξ as a function of α . The competition between layering and fluidized particles results in a maximum frustration length near impurities at $\alpha \approx 14$. A 3rd-order polynomial curve fit is used to estimate $\xi(\alpha)$.

constant at slightly higher values of $\langle |\psi_6| \rangle \approx 0.5\text{--}0.6$. This points to a competition between fluidisation of particles at highly curved surfaces and layer formation along moderately curved surfaces. Indeed confocal images reveal that close to a highly curved impurity surface the structure is fluidlike (Fig. 3c, $\alpha = 3$), whereas near larger impurities, particles start to orient along the impurity surface (Fig. 3d, $\alpha = 13$). This competition results in a maximum in ξ which we observe at $\alpha \approx 14$ (Fig. 3e). Unfortunately our data at large α are less abundant, since impurities of those sizes frequently had a strong deviation from a spherical shape. Nevertheless, the appearance of a maximum in $\xi(\alpha)$ is intuitively plausible, as two cases without frustration are *a priori* clear: $\alpha \rightarrow 1$ corresponds to a perfect crystal and $\alpha \rightarrow \infty$ represents a crystal next to a flat wall. The maximum is remarkably similar to the value of $\alpha = 10$ at which impurities start to spawn precritical crystal nuclei from their surface,³² a process for which the competition between layering and fluidisation is crucial as well.

The sum of the frustration lengths $\xi_1 + \xi_2$ of two nearby impurities represents their interaction range, and is used to

obtain the dimensionless impurity spacing, $\lambda = L/(\xi_1 + \xi_2)$, which is closely related to the pinning strength. For small λ a grain boundary should be strongly pinned: many defects have to nucleate to enable the grain boundary to migrate and anneal out. Moreover, overlap of the frustration lengths should allow the system to annihilate some defects, increasing grain boundary pinning. For larger λ , the pinning strength decreases, leading to fluctuations in grain boundary shapes and eventually the absence of pinned grain boundaries. The grain boundary shape, which we can extract from our data, therefore reflects the pinning strength. Indeed, a straight grain boundary is formed between two impurities when $\lambda = 1.4$ (Fig. 1a), whereas a curved grain boundary is observed for $\lambda = 2.0$ (Fig. 2b). To systematically investigate the correlation between the pinning strength (grain boundary shape) and the dimensionless impurity spacing λ , the area between impurities was divided into thin strips with length L and width w , as illustrated in Fig. 4a. By calculating the average orientational order in every strip $\langle |\psi_6| \rangle_{\text{strip}}$, a crystallinity profile is obtained such as in Fig. 4b. The minimum ($\langle |\psi_6| \rangle_{\text{min}}$) is more pronounced for straight grain boundaries and is therefore

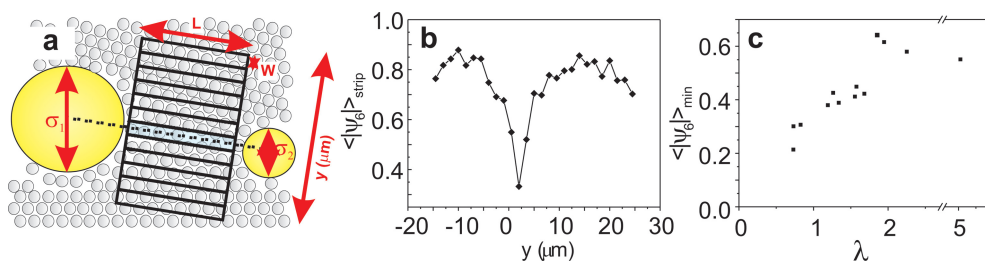


Fig. 4 The pinning strength as a function of the dimensionless impurity spacing λ . (a) Division of the area between the impurities into strips to obtain an average $\langle |\psi_6| \rangle$ value for each strip. (b) A representative crystallinity profile of a grain boundary, which clearly shows the minimum in $\langle |\psi_6| \rangle_{\text{strip}}$. The minimum reflects how straight the grain boundary is, that is, how strongly it is pinned. (c) $\langle |\psi_6| \rangle_{\text{min}}$ increases with the dimensionless impurity spacing λ , indicating that grain boundary pinning decreases with increasing λ . Roughly above $\lambda \approx 2 \langle |\psi_6| \rangle_{\text{min}}$ saturates and grain boundary pinning is not observed.

a measure for the grain boundary shape. A gradual rise in $\langle |\psi_6| \rangle_{\min}$ is observed with increasing λ (Fig. 4c), corresponding to a decreasing pinning strength. For roughly $\lambda \geq 2$ the correlation is lost and $\langle |\psi_6| \rangle_{\min}$ saturates. A clear transition between strong and weak pinning could not be identified and we have no grounds to expect this.

Our approach allows for an estimate on the circumstances under which grain boundary pinning is expected to occur. Considering grain boundary pinning at $\lambda = 1$ and $\xi = \alpha/2$, which is reasonable for not too large α as can be inferred from Fig. 3e, we find for the corresponding impurity volume fraction $\phi_i = (\alpha/2)^3 / (\alpha/2 + \xi)^3 = 1/8$. This corresponds to a system in which every impurity is surrounded by vanishingly small grains, which almost probes the crystal-to-glass transition for binary systems: indeed one scattering study reports a glassy system in such a regime.³³ Furthermore, it brings up an intriguing but subtle issue – at what point a polycrystalline structure becomes glassy? The situation becomes even more delicate in large size ratio binary systems ($\alpha > 3$) due to its many available binary crystal structures.³⁴ At lower impurity volume fractions (larger λ) the grain size is expected to increase as the number of pinned grain boundaries decreases. When the grain boundaries are not pinned, they should anneal out in an experiment where crystallisation is followed by a cycle of slight decreases and increases in volume fraction, an experiment that is feasible in a system of temperature-sensitive colloidal particles.¹⁶

Although we find the impurity-to-particle size ratio and the impurity-to-impurity spacing to be the central quantities in grain boundary pinning, there are other contributions that should be included in a more sophisticated description. First of all, the pinning strength is expected to depend on the orientational mismatch of the adjacent crystallites, *i.e.* interfacial tension. Secondly, the frustration length can be considered as a perturbation by the impurity on the hard sphere crystal, which may be different in truly monodisperse crystals and in systems at higher volume fractions, where interactions are more long ranged. Furthermore, it is not *a priori* clear whether these perturbations are additive: they are applied to crystals and are therefore clearly directionalized, which could result in an interaction range that is larger than $\xi_1 + \xi_2$. Interestingly, grain boundary pinning is indeed observed for $\lambda > 1$ (Fig. 4c), suggesting that the interaction range may actually be larger than sum of the two frustration lengths. Repeating our estimate for the impurity volume fraction, but now for $\lambda = 2$ and $\xi = \alpha/2$, we find $\phi_i = (\alpha/2)^3 / (\alpha/2 + 2\xi)^3 = 1/27$. Hence, even for impurity volume fractions as low as 1/27, effects of grain boundary pinning may be expected.

Conclusions

In conclusion, grain boundaries between impurities form due to the enhanced stability of the fluid phase during crystallisation. We have identified the impurity-to-particle size ratio and the impurity spacing as the key quantities for this process. We have introduced a frustration length, which characterizes up to what distance the crystal structure interacts with the impurity. The frustration length, which displays a maximum as a function of the impurity-to-particle size ratio, is used to define

a dimensionless impurity spacing which is directly related to the pinning strength. Grain boundaries are more strongly confined to the region between the impurities as the dimensionless impurity spacing decreases, *i.e.* the pinning strength increases. Our observations contribute to the fundamental understanding of grain boundary formation in doped materials and also provide valuable insights for a better control of the grain boundary density in material science and engineering applications.

Acknowledgements

We acknowledge Gilles Bosma, Hans Scherff and Esther Groeneveld for particle synthesis and David Nelson, Paul Millett, Bill van Meegen, Roland Roth and Dirk Aarts for valuable discussions. VWAdV acknowledges the “Nederlandse Organisatie voor Wetenschappelijk Onderzoek (NWO)” for financial support. The work of ECMV is supported by NanoNed, a nanotechnology program of the Dutch Ministry of Economic Affairs. RPAD acknowledges the Alexander von Humboldt Foundation for financial support.

References

- 1 J. P. Hirth and J. Lothe, *Theory of dislocations*, Wiley, New York, 1982, 2nd edn.
- 2 S. Yip, *Nature*, 1998, **391**, 532.
- 3 R. Phillips, *Crystals, defects and microstructure*, Cambridge University Press, Cambridge, 2001.
- 4 H. Gleiter, *Acta Mater.*, 2000, **48**, 1.
- 5 E. O. Hall, *Proc. Phys. Soc. Lond. B*, 1951, **64**, 747.
- 6 N. J. Petch, *J. Iron Steel Inst.*, 1953, **174**, 25.
- 7 S. E. Offermans, N. H. van Dijk, J. Sietsma, S. Grigull, E. M. Lauridsen, L. Margulies, H. F. Poulsen, M. T. Rekveldt and S. van der Zwaag, *Science*, 2002, **298**, 1003.
- 8 Q. H. Wei and X. L. Wu, *Phys. Rev. E*, 2004, **70**, 020401(R).
- 9 P. C. Millett, R. P. Selvam and A. Saxena, *Acta Mater.*, 2007, **55**, 2329.
- 10 G. Duscher, M. F. Chisholm, U. Alber and M. Rühle, *Nature Mater.*, 2004, **3**, 621.
- 11 V. Randle and B. Ralph, *Acta Metall.*, 1986, **34**, 891.
- 12 J. J. Hoyt, *Acta Metall. Mater.*, 1991, **39**, 2091.
- 13 P. N. Pusey and W. van Meegen, *Nature*, 1986, **320**, 340.
- 14 V. W. A. de Villeneuve, R. P. A. Dullens, D. G. A. L. Aarts, E. Groeneveld, J. H. Scherff, W. K. Kegel and H. N. W. Lekkerkerker, *Science*, 2005, **309**, 1231.
- 15 U. Gasser, E. R. Weeks, A. Schofield, P. N. Pusey and D. A. Weitz, *Science*, 2001, **292**, 258.
- 16 A. M. Alsayed, M. F. Islam, J. Zhang, P. J. Collings and A. G. Yodh, *Science*, 2005, **309**, 1207.
- 17 P. Schall, I. Cohen, D. A. Weitz and F. Spaepen, *Science*, 2004, **305**, 1944.
- 18 P. Lipowsky, M. J. Bowick, J. H. Meinke, D. R. Nelson and A. R. Bausch, *Nature Mater.*, 2005, **4**, 407.
- 19 A. Pertsinidis and X. S. Ling, *Nature*, 2001, **413**, 147.
- 20 M. J. Mills, *Mater. Sci. Eng., A*, 1993, **166**, 35.
- 21 K. L. Merkle, *Interface Sci.*, 1995, **2**, 311.
- 22 D. A. Muller and M. J. Mills, *Mater. Sci. Eng., A*, 1999, **260**, 12.
- 23 V. W. A. de Villeneuve, D. Verboekend, R. P. A. Dullens, D. G. A. L. Aarts, W. K. Kegel and H. N. W. Lekkerkerker, *J. Phys.: Condens. Matter*, 2005, **17**, S3371.
- 24 R. P. A. Dullens, V. W. A. de Villeneuve, M. C. D. Mourad, A. V. Petukhov and W. K. Kegel, *Eur. Phys. J. Appl. Phys.*, 2008, **44**, 21.
- 25 R. P. A. Dullens, D. G. A. L. Aarts and W. K. Kegel, *Proc. Natl. Ac. Sci. USA*, 2006, **103**, 529.
- 26 A. Yethiraj and A. van Blaaderen, *Nature*, 2003, **421**, 513.
- 27 J. C. Crocker and D. G. Grier, *J. Colloid Interface Sci.*, 1996, **179**, 298.
- 28 P. C. Millett, R. P. Selvam, S. Bansal and A. Saxena, *Acta Mater.*, 2005, **53**, 3671.

-
- 29 D. R. Nelson, *Defects and geometry in condensed matter physics*, Cambridge University Press, Cambridge, 2002.
- 30 P. M. König, P. Bryk, K. Mecke and R. Roth, *Europhys. Lett.*, 2005, **69**, 832.
- 31 C. S. Smith, *Trans. AIME*, 1948, **175**, 15.
- 32 A. Cacciuto, S. Auer and D. Frenkel, *Nature*, 2004, **428**, 404.
- 33 A. Imhof and J. K. G. Dhont, *Phys. Rev. Lett.*, 1995, **75**, 1662.
- 34 J. V. Sanders and M. S. Murray, *Phil. Mag. A*, 1980, **42**, 721.